1
Phase Behavior of Rod-Like Viruses and Virus–Sphere Mixtures

Zvonimir Dogic and Seth Fraden

Abstract

An overview is given of the experimental work on the liquid crystalline phase behavior of semi-flexible viruses in an aqueous solution. We start by briefly summarizing the theoretical work of Onsager which describes the isotropic-nematic phase transitions of perfectly rigid rods. Extensions of the Onsager theory to the case of semi-flexible and charged rods are presented. In the first part of the review we focus on the phase behavior of a pure solution of semi-flexible virus *fd*. With increasing concentration *fd* form isotropic, cholesteric and smectic phase. In the limit of high ionic strength the agreement between the Onsager theory and experiments on the isotropic-nematic phase of *fd* virus is quantitative. The discrepancies at low ionic strength strongly hint at a need to rigorously incorporate electrostatic interactions into phase behavior of rigid rods. In the second part of the review we focus on the phase behavior of mixtures of rods with either hard spheres or flexible polymers. Amongst others we described a number of novel phases observed in these mixtures such as a lamellar phase, columnar phase, colloidal membranes and surface induced smectic phase. These structures are still very poorly understood and there is a clear need for the theoretical work explaining their stability.

1.1
Introduction

The reasons physicists give for studying colloids are varied. Our initial motivation was that colloids can serve as model experimental systems to study simple fluids because, with careful preparation, colloids approximate hard particles. Numerous studies have investigated the phase behavior, structure,

Soft Matter, Vol. 2: Complex Colloidal Suspensions. Edited by G. Gompper and M. Schick

ISBN: 3-527-31369-9

and macroscopic viscoelastic properties of suspensions of spherical colloids (Poon and Pusey 1995). Far less studied have been colloids of anisotropic shape, in spite of their long-recognized similarity to liquid crystals. Counterintuitively, hard-rod fluids are theoretically simpler systems to understand than hard spheres (Forsyth et al. 1978). This surprising fact was first recognized by Onsager (1949), who realized that the isotropic–nematic (I–N) transition in the rod-like colloid tobacco mosaic virus (TMV) occurred at such low concentrations that only two-body interactions were necessary in order to quantitatively explain the I–N phase transition. In fact, in the limit of long thin rods, Onsager's theory becomes exact. This is in contrast to the theory of phase transitions of hard spheres, for which no exact results exist (in three dimensions).

For some years, the Complex Fluids Group at Brandeis has studied the liquid-crystalline behavior of suspensions of TMV (Fraden et al. 1985; Hurd et al. 1985; Wen and Meyer 1987; Oldenbourg et al. 1988; Fraden et al. 1989; Meyer 1990; Fraden et al. 1993; Wang et al. 1994; Fraden 1995; Adams and Fraden 1998) and filamentous phage *fd* (Tang and Fraden 1993; Tang and Fraden 1995; Fraden 1995; Tang and Fraden 1996; Dogic and Fraden 1997; Adams et al. 1998; Dogic et al. 2000; Dogic and Fraden 2001; Grelet and Fraden 2003; Dogic 2003; Purdy et al. 2003; Purdy and Fraden 2004a; Purdy and Fraden 2004b; Purdy et al. 2005). TMV is a beautiful colloidal rod (Kreibig and Wetter 1980; Wetter 1985). It is completely rigid and forms isotropic, nematic, smectic and colloidal crystalline phases. However, TMV is difficult to work with. One must cultivate tobacco plants, infect them with virus, harvest the crop, extract the virus – which takes months – and, in addition, all this must be done with care to preserve the monodispersity of the virus. Physics graduate students rebel at the thought of producing enough virus for a PhD thesis! Without an abundant source of TMV, studies of its phase behavior are impracticable.

So our laboratory switched from TMV to the semi-flexible bacteriophage *fd*, which also forms several liquid-crystalline phases: isotropic, cholesteric, and smectic, but not colloidal crystals. Because *fd* infects bacteria, growing *fd* is relatively quick and easy. Furthermore, genetic engineering of *fd* is well established, and we have produced mutants of varying length and charge.

This chapter describes the phase behavior of *fd* virus suspensions. First, we present our results on *fd* alone. The results obtained up to 1995 are summarized in another review article (Fraden 1995). While theory and experiment are in agreement for the isotropic–cholesteric phase transition for suspensions with high salt concentrations used to screen long-range electrostatic repulsion, theoretical explanations of all other phases fail. We see a quantitative discrepancy between theory and experiment for the nematic phase at low ionic strength, and multiple quantitative and qualitative breakdowns of the

theory of the smectic phase. Also, we have not even a clue of why a cholesteric phase is observed in *fd*, but a nematic in a closely related species, *pf1*, which has a nearly identical atomic structure (Grelet and Fraden 2003). Second, we present results on mixtures of the viral rods with spherical colloids or spherical polymers. Some of the phase behavior, such as depletion-induced phase separation, was as anticipated. But an astounding array of unexpected results was also observed. A laundry list includes microphase separation of rods and spheres into columnar, cubic, and lamellar structure; isolated colloidal membranes consisting of a sheet of rods and stabilized via protrusion forces; and a quasi-two-dimensional smectic phase that exists on the isotropic–nematic interface that plays a key role in phase separation kinetics. While originally we were motivated to study virus suspensions because they are model systems of simple fluids, now we are motivated by a spirit of exploration driven by the expectation that more unexpected results will follow the ones described below.

1.2 Entropy-Driven Ordering Within the Second Virial Approximation

In the first part of this chapter we briefly review the theoretical work describing liquid-crystalline phase transitions in colloidal rods. This is not meant to be exhaustive. For more detailed theoretical accounts, the reader is referred to recent review articles (Stephen and Straley 1974; Odijk 1986; Vroege and Lekkerkerker 1992) and the original article by Onsager (1949).

The majority of studies of the ordering transitions in hard-particle fluids belong to a class of theories called density-functional theories (DFTs) (Hansen and McDonald 1986). The simplest version of DFT takes into account the interactions between particles at the level of second virial approximation. The free energy of a hard-particle fluid is then

$$\frac{F}{k_{\mathrm{B}}T} = \int_V \mathrm{d}\boldsymbol{r}\, \rho(\boldsymbol{r}) \ln[\rho(\boldsymbol{r})] - \tfrac{1}{2} \int_V \mathrm{d}\boldsymbol{r}_1 \int_V \mathrm{d}\boldsymbol{r}_2\, \rho(\boldsymbol{r}_1)\rho(\boldsymbol{r}_2)\beta(\boldsymbol{r}_1, \boldsymbol{r}_2) \qquad (1.1)$$

where k_{B} is the Boltzmann constant, T is the absolute temperature, $\rho(\boldsymbol{r})$ denotes the density of particles, $\boldsymbol{r}_1$ and $\boldsymbol{r}_2$ are vectors denoting the position and/or orientation of two particular particles, and $\beta(\boldsymbol{r}_1, \boldsymbol{r}_2)$ is the Meyer–Meyer overlap function. Its value equals -1 if there is any overlap between two hard particles located at $\boldsymbol{r}_1$ and $\boldsymbol{r}_2$; otherwise its value is equal to zero. This expression has been used for a variety of cases to study entropy-induced ordering in hard-particle fluids. Onsager (1949) was the first to show that Eq. (1.1) is essentially exact for isotropic spherocylinders when $L/D_{\mathrm{sc}} \to \infty$, where L is the length and D_{sc} is the diameter of the spherocylinder. As

the aspect ratio of spherocylinders is increased, the third and higher virial coefficients become negligible.

The second virial theory also predicts a stable smectic phase in a solution of perfectly aligned spherocylinders as well as for spherocylinders with both positional and orientational degrees of freedom (Hosino et al. 1979; Mulder 1987; van Roij et al. 1995; van der Schoot 1996). However, to describe the suspensions quantitatively at the densities of the nematic–smectic (N–S) phase transition, it is necessary to include higher virial coefficients in the free-energy expression. For perfectly aligned spherocylinders, inclusion of the third and fourth virial coefficients into the free energy results in theoretical predictions for the N–S transitions that are in quantitative agreement with simulation results. The calculations that consider ordering transitions using only second virial coefficients are uncontrolled approximations, unless it can be shown that higher virial coefficients are negligible, as is the case of the Onsager treatment of the I–N phase transition.

In any hard-particle fluid, due to the simplicity of the interaction potential, the energy of any allowed configuration is simply proportional to $nk_{\mathrm{B}}T$, with n being the number density of particles. Due to this simple fact, the minimum of the free energy of a hard-particle fluid $F = E - ST = T(\alpha - S)$ (α is a constant) is equivalent to the maximum of the entropy. Furthermore, the resulting phase diagram is temperature-independent (athermal) because both α and S are independent of temperature. Ordering transitions in hard-particle fluids are still possible because the expression for entropy, or equivalently free energy, splits into two parts. The first integral in Eq. (1.1) is the ideal part of the free energy and always attains a minimum value for the uniform probability distribution $\rho(\boldsymbol{r}) = \text{constant}$. Therefore, this contribution to the total free energy always suppresses an ordering transition. The second integral in Eq. (1.1) represents the second virial approximation for the interaction free energy, which is proportional to the excluded volume, and under certain circumstances is lower for an ordered state. Therefore, the interaction part of the free energy drives the system toward ordering. The actual location of the ordering transition is determined from the competition between the ideal and interaction contributions to the total free energy. In this section, we briefly review the theoretical description of phase transitions that can be described using Eq. (1.1) for pure hard rods.

1.2.1
Isotropic–Nematic Phase Transition Within the Second Virial Approximation

The density functional of the sort shown in Eq. (1.1) was first used in a seminal paper by Onsager (1949). He was seeking to explain the formation of the nematic phase in solutions of rod-like tobacco mosaic virus (TMV), inorganic

needles of vanadium pentoxide, and discs of bentonite. These transitions were found to occur at very low volume fraction (Zocher 1925; Bawden et al. 1936).

In the Onsager theory, the system is assumed to be spatially uniform and therefore it is assumed that $\rho(\boldsymbol{r}, \Omega) = (N/V) f(\Omega)$, where Ω is the solid angle describing the orientation of the spherocylinder, N is the number of rods, and V is the volume of the system. Since $f(\Omega)$ indicates the probability that a rod is pointing at a solid angle Ω, it should be normalized as follows:

$$\int f(\Omega)\,\mathrm{d}\Omega = 1 \tag{1.2}$$

Using this information, it is possible to recast Eq. (1.1) into an Onsager free-energy functional for a solution of rod-like molecules:

$$F = \log\left(\frac{N}{V}\right) + \int f(\Omega)\log[4\pi f(\Omega)]\,\mathrm{d}\Omega$$
$$-\frac{1}{2}\frac{N}{V}\int\int \beta(\Omega,\Omega')f(\Omega)f(\Omega')\,\mathrm{d}\Omega\,\mathrm{d}\Omega' \tag{1.3}$$

The function $\beta(\Omega, \Omega')$ is the excluded volume of the spherocylinder with orientation Ω' due to the presence of another spherocylinder with orientation Ω. For two spherocylinders it is given by

$$\beta(\Omega,\Omega') = \beta(\gamma) = -2L^2 D_{\mathrm{sc}}\sin\gamma - 2\pi D_{\mathrm{sc}}^2 L - \tfrac{4}{3}\pi D_{\mathrm{sc}}^3 \tag{1.4}$$

where γ is the relative angle between the two spherocylinders. For spherocylinders with a large aspect ratio, the first term in Eq. (1.4) dominates, and it can be shown that the contribution of the other terms is of the same order as the contribution of the third virial coefficient. Therefore, it is often assumed that $\beta(\gamma) = -2L^2 D_{\mathrm{sc}}\sin\gamma$.

By using this approximation and variational calculus to minimize Eq. (1.3) with respect to the distribution function $f(\Omega)$, one obtains the following integral equation:

$$\log[4\pi f(\theta)] = \lambda - \frac{8\rho}{\pi}\int \sin\theta\, f(\theta)\,\mathrm{d}\theta \tag{1.5}$$

where $\rho = \frac{1}{4}\pi L^2 D_{\mathrm{sc}} N/V$ and λ is a constant determined through normalization of the constraint in Eq. (1.2). This integral equation cannot be solved analytically. However, it has been solved using two different numerical procedures, which yield almost identical results (Herzfeld et al. 1984; Lekkerkerker et al. 1984). Once the probability distribution function is known, it is easy to

calculate the nematic order parameter (S_2) using the following relation:

$$S_2 = 2\pi \int_0^{\pi} [\tfrac{3}{2}\cos\theta - \tfrac{1}{2}] f(\theta) \sin\theta \, \mathrm{d}\theta \tag{1.6}$$

In this equation we assume that the orientational distribution function is uniaxial and therefore $f(\Omega) = f(\theta)$, where θ is the angle between the orientation of a specific rod and the nematic director. The value of the nematic order parameter varies between 0 and 1, with $S_2 = 0$ describing a perfectly isotropic solution and $S_2 = 1$ describing a perfectly aligned nematic phase. Although the numerical solution of Eq. (1.5) yields the most accurate results, it is also possible to proceed from Eq. (1.3) by assuming a form of the orientational distribution function, such as

$$f(\alpha, \cos\theta) = \frac{\alpha \cosh(\alpha \cos\theta)}{4\pi \sinh\alpha} \tag{1.7}$$

Using this ansatz, first introduced by Onsager, and evaluating the integrals for the case of hard rods, Onsager obtained an expression for the free energy as a function of dimensionless concentration ρ and orientation parameter α:

$$\begin{aligned} F(\alpha, \rho) &= \rho \log \rho + \sigma(\alpha)\rho + \xi(\alpha)\rho^2 \\ \sigma(\alpha) &= \log\left(\frac{\alpha \cosh\alpha}{4\pi \sinh\alpha}\right) - 1 + \frac{\arctan(\mathrm{e}^{\alpha}) - \arctan(\mathrm{e}^{-\alpha})}{\sinh\alpha} \\ \xi(\alpha) &= \frac{2I_2(\alpha)}{\sinh^2\alpha} \end{aligned} \tag{1.8}$$

The advantage of assuming the probability distribution (1.7) is the analytical expression for the free energy (1.8). The most convenient variable to formulate the Onsager theory is the dimensionless concentration

$$\rho = B_2^{\mathrm{iso}} \frac{N}{V} = \frac{\pi}{4} L^2 D_{\mathrm{sc}} \frac{N}{V} = \frac{L}{D_{\mathrm{sc}}} \phi \tag{1.9}$$

where ϕ is the volume fraction of rods and $B_2^{\mathrm{iso}} = (\pi/4) L^2 D_{\mathrm{sc}}$ is the second virial coefficient for a suspension of hard rods in an isotropic solution. By performing a stability analysis of the Onsager equation, Kayser and Raveche (1978) found that the isotropic phase becomes unstable toward orientational fluctuations when $\rho = 4$. It follows that, within the Onsager theory, the volume fraction of hard rods at the I–N transition scales as $\phi = 4D_{\mathrm{sc}}/L$. Therefore, for long thin rods, the volume fraction of the I–N transition is small and the virial theory, which is an expansion of the free energy in density, becomes

accurate at the level of the second virial coefficient. Numerical calculations of the second and third virial coefficients indicate that the Onsager theory is quantitatively correct for rods with $L/D_{\mathrm{sc}} > 100$ (Frenkel 1988).

However, the second-order transition predicted by the stability analysis is preempted by a first-order phase transition. Minimizing the Onsager free energy with respect to the orientational distribution function numerically and subsequently solving the coexistence equations yields the following concentration of the coexisting isotropic and nematic phases:

$$\rho_{\mathrm{iso}} = 3.289, \quad \rho_{\mathrm{nem}} = 4.192, \quad S_2 = 0.7922 \tag{1.10}$$

These results were obtained by Herzfeld et al. (1984), Lekkerkerker et al. (1984), and Chen (1993). The Onsager trial function (Eq. 1.7) yields the following coexistence concentrations:

$$\rho_{\mathrm{iso}} = 3.339, \quad \rho_{\mathrm{nem}} = 4.487, \quad S_2 = 0.848 \tag{1.11}$$

By comparing the accurate numerical result from Eq. (1.5) with the Onsager approximation (Eq. 1.8), we observe a difference in both the coexistence concentrations at the I–N phase transition and the nematic order parameter (S_2) of the nematic phase.

1.2.2 Extension of Onsager Theory to Charged Rods

The Onsager theory outlined in the previous section can be extended to the experimentally important case of charge-stabilized rods. The first treatment of the I–N phase transition of charged rods can be found in the original paper by Onsager (1949) and was elaborated by Stroobants et al. (1986). Besides the hard-core repulsive interaction, charged rods have a long-range repulsive interaction of the following form:

$$\frac{U_{\mathrm{el}}(x)}{k_{\mathrm{B}}T} = \frac{A' \, \mathrm{e}^{-\kappa(x - D_{\mathrm{sc}})}}{\sin\gamma} \tag{1.12}$$

where x is the closest distance between two charged rods, A' is the proportionality constant obtained by solving the Poisson–Boltzmann equation, κ^{-1} is the Debye screening length, and γ is the angle between two rods. In the case of charged rods, there are contributions to the second virial coefficient from both the hard-core excluded-volume interaction and the long-range electrostatic repulsion interaction. These two contributions can be calculated separately. Integrating the interaction potential over a uniform orientational

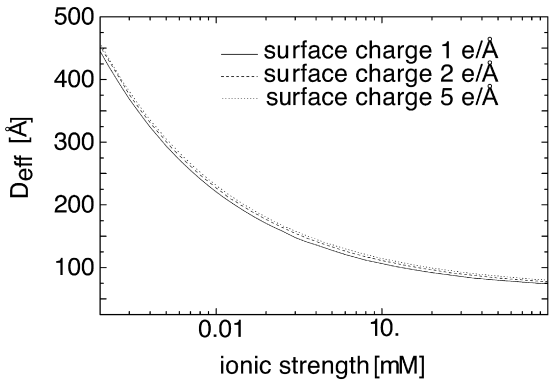

Fig. 1.1 The effective diameter for a charged rod calculated from Eq. (1.13) for a range of ionic strengths. The hard-rod diameter $D_{\rm bare} = 66$ Å is that of the *fd* virus. Due to the highly nonlinear nature of the Poisson–Boltzmann equation, the value of $D_{\rm eff}$ barely changes as the surface charge varies from $1\ {\rm e}^-/$Å to $10\ {\rm e}^-/$Å. Experiments indicate that the surface charge is about $2\ {\rm e}^-/$Å at pH 8.0 (Zimmermann et al. 1986). (Taken from Tang and Fraden, 1996).

distribution function that describes the isotropic phase, we obtain the following expression for the second virial coefficient of charged rods (see Fig. 1.1):

$$B_2^{\rm iso} = \tfrac{1}{4}\pi L^2 D_{\rm eff} = \tfrac{1}{4}\pi D L^2 + \tfrac{1}{4}\pi\kappa^{-1}L^2(\ln A' + C_E + \ln 2 - \tfrac{1}{2}) \quad (1.13)$$

where $D_{\rm eff} = (\ln A' + C_E + \ln 2 - \frac{1}{2})/\kappa$. It follows that the thermodynamics of charged rods in the isotropic suspension will be equivalent to the thermodynamics of thicker hard rods with effective diameter $D_{\rm eff}$.

However, if the interaction potential is integrated over an anisotropic distribution function, then the relationship given by Eq. (1.13) is no longer exact. The reason for this is that the electrostatic energy is lower for perpendicular rods than for parallel rods. Therefore, the charge effectively destabilizes the nematic phase by shifting the I–N transition to higher concentrations and reducing the order parameter of the nematic phase coexisting with the isotropic phase. However, most biopolymers (including *fd* virus) are highly charged, in which case it turns out that the electrostatic "twisting" effect is insignificant compared to the excluded-volume interactions (Stroobants et al. 1986; Tang and Fraden 1995). Therefore, from now on we approximate $D_{\rm eff}$ in the nematic phase by $D_{\rm eff}$ of the isotropic phase. This is reasonable for coexisting phases, but we expect this approximation to get progressively worse with increasing concentration.

1.2.3 Extension of Onsager Theory to Semi-Flexible Rods

Semi-flexible rods are characterized by their persistence length, which is the length along the contour of the chain after which the local tangents become uncorrelated. The effect of semi-flexibility on the isotropic–nematic phase transition was first considered by Khokhlov and Semenov (1982). For semi-flexible rods, besides orientational and translational entropy, it is also necessary to take into account the internal configurations of the semi-flexible chain. This modifies the orientational entropy term in Eq. (1.1), while the excluded-volume term between rod-like segments is still treated as in the Onsager theory for rigid rods. The resulting expression for the free energy has been solved analytically in the limit of almost rigid rods ($P \gg L$) and very flexible rods ($L \ll P$) (Khokhlov and Semenov 1981; Khokhlov and Semenov 1982). It is possible to interpolate empirically between these two solutions and obtain a numerical approximation for the configurational entropy of rods with arbitrary persistence length, as was done by Hentschke (1990), Odijk (1986), and DuPre and Yang (1991). This interpolated expression can be combined with the Onsager approximation for the orientational distribution to obtain analytical results for the I–N phase transition of semi-flexible rods. In Fig. 1.2 these results are compared to accurate numerical solutions of the Khokhlov–Semenov free energy due to Chen (1993).

From Fig. 1.2a we conclude that increasing flexibility destabilizes the nematic phase by displacing the I–N transition to higher volume fractions. Increasing the flexibility also drastically reduces the concentration difference between the coexisting isotropic and nematic phases (figure not shown) and the order parameter of the nematic phase (Fig. 1.2b). The Onsager approximation (Eq. 1.7) for the orientational distribution function (ODF) qualitatively agrees with the accurate numerical results due to Chen. It is important to note that the agreement between these approximations for the location of the phase transition (Fig. 1.2a) is much better than for the order parameter of the coexisting nematic phases (Fig. 1.2b). This indicates that measuring the order parameter is a more sensitive test of the theory for the I–N phase transition.

Chen compares his numerical solution to the analytical solution of Khokhlov and Semenov, who also use the Onsager approximation for the ODF. This comparison in Chen's paper seems much better than what is shown in Fig. 1.2. The reason for this is that Khokhlov and Semenov, besides using the Onsager approximation for the ODF, also approximate the excluded volume $\xi(\alpha)$ by expanding it in powers of α. These two approximations fortuitously cancel each other, and the final result seemingly agrees better with the numerical solution.

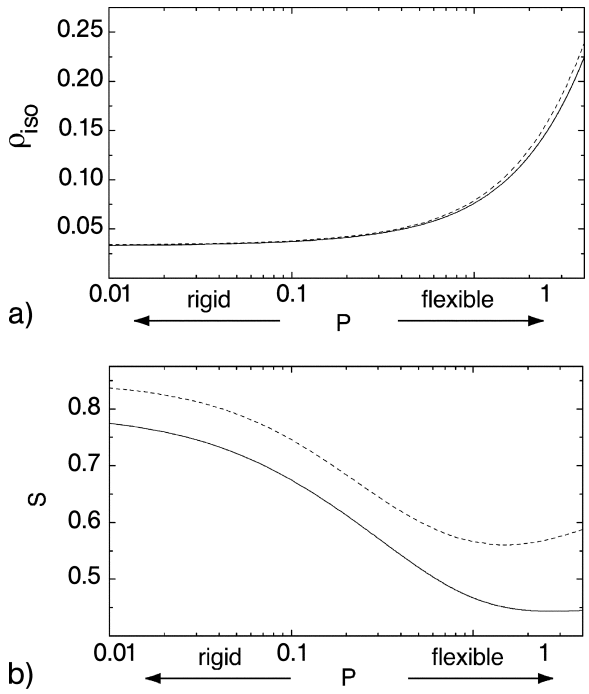

Fig. 1.2 (a) Concentration [$\rho_{\rm iso} = (4/\pi)L^2 D_{\rm sc}(N/V)$] and (b) order parameter (S_2) of the nematic phase coexisting with the isotropic phase as a function of the flexibility of the particle $P = L/l_{\rm p}$. The full lines are the exact numerical results within the second virial approximation due to Chen (1993), while the dashed lines are results obtained by using the Onsager approximation for the orientational distribution function (Eq. 1.7). In both parts the aspect ratio of the rods is fixed at 100 and the persistence length $l_{\rm p}$ varies from infinity to 25.

1.2.4
Extension of Onsager Theory to Rods With Finite Aspect Ratio Using Scaled Particle Theory

The scaled particle theory (SPT) of hard rods was developed by Cotter and Wacker (1978) and Cotter (1979). The main advantage of the scaled particle theory is that it takes into account third and all higher virial coefficients in an approximate way. Therefore, this theory should be more adequate at describing the data at higher concentration of rods or equivalently rods with lower $L/D_{\rm sc}$ ratios. We note that the expression for the free energy reduces to the Onsager second virial approximation for very long rods. For spherical particles, the SPT free energy reduces to the Percus–Yevick free energy for hard spheres.

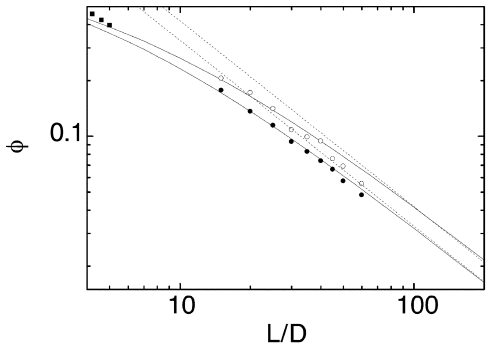

Fig. 1.3 The I–N coexistence concentrations as a function of the aspect ratio $(L/D_{\rm sc})$ as predicted by the scaled particle theory for rigid rods (full lines) and as predicted by a theory that only includes the second virial coefficient (dashed lines). The circles are the results of computer simulations (Bolhuis and Frenkel 1997). The filled squares at low $L/D_{\rm sc}$ represent results from the same work but the coexistence width was too narrow to be measured. The coexistence is plotted in terms of real volume fraction $\phi = \frac{1}{6}\pi D_{\rm sc}^3 + \frac{1}{4}LD_{\rm sc}^2\pi$, while the total aspect ratio including the hemispheres is $L/D_{\rm sc} + 1$.

The scaled particle expression accounts for higher virial coefficients in an approximate way. Comparing the SPT prediction for the I–N phase transition with the solution obtained through the second virial approximation provides a way to establish the range of $L/D_{\rm sc}$ ratios for which the second virial approximation is quantitatively valid. The results are shown in Fig. 1.3. At $L/D_{\rm sc} = 45$ the second virial approximation yields I–N coexistence concentrations that are 10% different from the scaled particle result. We conclude that for rods with $L/D_{\rm sc} > 75$ the second virial approximation quantitatively describes the I–N transitions in hard rods. Currently available computer simulation results agree very well with the scaled particle theory (Bolhuis and Frenkel 1997; Kramer and Herzfeld 1998).

1.2.5
Nematic–Smectic Phase Transition Within the Second Virial Approximation

Here we review the interplay between the ideal and interaction contributions to the free energy that are responsible for the formation of the smectic phase in parallel hard rods. From the second virial approximation (Eq. 1.1), we can easily find the free-energy difference between a weakly ordered smectic and a uniform nematic state (Mulder 1987):

$$\begin{aligned}\delta F &= F_{\rm layered} - F_{\rm uniform} \\ &= F(n + a\cos(kz)) - F(n) = n + 8n^2 j_0(k)\end{aligned} \tag{1.14}$$

A positive free-energy difference $\delta F(n,k) > 0$ implies that at volume fraction n and wavevector k the nematic phase has the lowest free energy and therefore is the equilibrium phase. On the other hand, at values of n_c and k_c that satisfy the equation $\delta F(n_c, k_c) = 0$ the system becomes unstable toward smectic fluctuations since they do not cost any energy to create. We identify n_c and k_c as the critical volume fraction and critical wavevector of the second-order nematic–smectic phase transition.

It is important to note that the first term in Eq. (1.14) originates from the ideal part of the free energy in Eq. (1.1), while the second term in Eq. (1.14) originates from the interaction part of the free energy in Eq. (1.1). We observe that the difference in the ideal part of the free energy between the layered and uniform phase is always positive and given by $\delta F \propto n$. Therefore, the ideal part of the free energy always suppresses the ordering transition as expected. On the other hand, the difference in the interaction part of the free energy between the uniform and layered phase is given by $\delta F \propto n^2 j_0(k)$. Since this part of the free-energy difference scales as n^2, for high enough volume fraction of rods and for specific values of wavevector k this term is negative and large enough to drive the system toward the smectic phase. Considering the highly approximate nature of the theory, the conditions $n_c = 0.575$ and $k_c = 2\pi/1.398L$ obtained for the nematic–smectic phase transition compare favorably to the results of the computer simulations of parallel rods $n_c = 0.43$ and $k_c = 2\pi/1.27L$ (Frenkel et al. 1988). Inclusion of the third virial coefficient brings the theoretical prediction for the N–S transition closer to what is observed in simulations (Mulder 1987).

The above simple model suggests a physical picture of the excluded-volume effects responsible for the formation of a smectic phase first introduced by Wen and Meyer (1987). A spatially uniform nematic phase results in a very inefficient packing of rods, as shown in Fig. 1.4a. In such a state the ideal

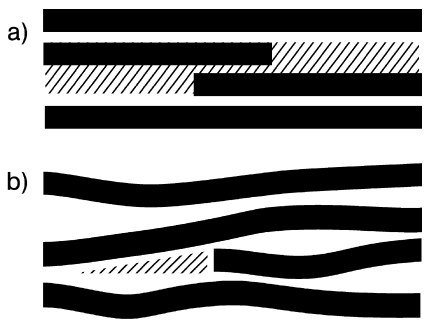

Fig. 1.4 A schematic illustration of the excluded-volume interaction in a dense suspension of aligned rods for the case of (a) rigid rods and (b) semi-flexible rods. (From Tkachenko, 1996).

part of the free energy attains its minimum value while the interaction part does not. The reason for this is that the nematic phase is under the constraint of uniform packing, and thus the excluded volume between any two rods is eight times the volume of a single rod, since rods are allowed to approach each other from any direction. One way to decrease the excluded volume is to impose a smectic-like periodic density modulation. Then the probability of two rods approaching each other along their axial direction will decrease, while the probability of sideways approach will increase. For example, in an extreme case where the probability distribution of the centers of rods consists of very sharp delta-like functions spaced at distances slightly longer than the rod length, rods are allowed to approach each other only sideways and overlap between the ends of the rods is completely forbidden. Consequently, the excluded volume between two rods will be half the value of the excluded volume for a uniform density distribution. For this simple reason, the value of the interaction part of the free energy decreases with increasing order in Eq. (1.14). The actual volume fraction of the ordering transition and the resulting density distribution $\rho(\boldsymbol{r})$ is therefore determined by the competition between the ideal and interaction parts of the free energy given in expression (1.1). The treatment of the nematic–smectic phase transition of the second virial approximation was also extended to the case of rods with orientational freedom (van Roij et al. 1995). In this case the calculation becomes much more involved.

It is easy to extend the above argument to consider the influence of flexibility on the nematic–smectic phase transition (Tkachenko 1996; van der Schoot 1996). Experimentally, it is found that flexibility acts to stabilize the nematic phase and destabilize the smectic phase (Dogic and Fraden 1997). As was first noticed by Tkachenko (1996), in the case of perfectly aligned rigid-rod nematics the only way to fill the space created by the end of a rod is to place another rod above it, as shown in Fig. 1.4a. In the case of a nematic solution of semi-flexible rods, it is possible for other molecules to occupy space around the end of a particular molecule by deflecting around its end, as shown in Fig. 1.4b. This results in more efficient packing of semi-flexible rods in the nematic state, which in turn leads to the suppression of the nematic–smectic phase transition. This picture of the effect of flexibility on the nematic–smectic phase transition has been confirmed using computer simulations (Polson 1997).

1.2.6
Phase Behavior of a Binary Mixture of Hard Particles

Recently the second virial approximation has also been extended to study ordering and demixing transitions in binary mixtures of hard rods (Koda and

Kimura 1994; Cui and Cheng 1994; van Roij 1994; Sear and Jackson 1995; Sear and Mulder 1996; van Roij 1996; van Roij and Mulder 1996; Dijkstra and van Roij 1997; van Roij et al. 1998). In many of these cases it is not obvious if terminating the free-energy expansions at a second virial level is sufficient to describe the phase diagram of a binary mixture. For example, it was recently shown that, although Onsager theory quantitatively describes the I–N phase transitions of rods, it fails to predict even the qualitative features of a binary mixture of rods with two different diameters (Purdy et al. 2005). In other cases, such as a mixture of perfectly aligned spherocylinders and hard spheres, the second virial theory predicts the right qualitative features, as has been verified by computer simulations for the lamellar phase, but fails to describe the columnar phase (Adams et al. 1998). Expressions for the stability matrix for a binary mixture of parallel spherocylinders and spheres are given in Koda et al. (1996) and Dogic et al. (2000).

1.3 Experimental Phase Diagram of an *fd* Virus Suspension

Theory and simulation indicate that, with increasing concentration, rod-like particles will form isotropic, nematic, and smectic phases (Hosino et al. 1979; Mulder 1987; Wen and Meyer 1987; Frenkel et al. 1988; Bolhuis and Frenkel 1997). The columnar phase turns out to be metastable with respect to the smectic phase for all aspect ratios and rod concentrations (Bolhuis and Frenkel 1997). So far, the only experimental systems whose phase behavior agrees with theoretical predictions are colloidal suspensions of the viruses *fd*, *pf1*, and TMV, and inorganic β-FeOOH rods (Maeda and Maeda 2003). This is due to the fact that Nature makes all viruses identical to each other. This results in a colloidal suspension of very high monodispersity, much higher than what can be achieved with current synthetic methods. Recently, using a combination of recombinant DNA technology and traditional chemical methods, it has been possible to prepare monodisperse poly(benzyl L-glutamate) (PBLG) polymers. Although these polymers are not available in large quantities, they were reported to form a smectic phase (Yu et al. 1997). This is a potentially powerful technique to create novel liquid crystals. While the present chapter focusses on the fundamental aspects of the phase behavior of rods and rod–sphere mixtures, individual viruses and virus assemblies might become technologically useful materials. In this respect, the recent work by Belcher's group seems promising (Lee et al. 2002).

In this chapter we focus on the phase behavior of the rod-like bacteriophage *fd* and its closely related M13. The phase behavior of another class of anisotropic colloids composed of minerals has recently been reviewed else-

where (Gabriel and Davidson 2003). The phase behavior of polymeric liquid crystals such as PBLG is reviewed in Sato and Teramoto (1994). Historically, the first observation of the nematic liquid-crystalline phase of *fd* was reported in the study by Lapointe and Marvin (1973). Shortly thereafter a smectic phase was also reported in a little noticed paper (Booy and Fowler 1985).

We note that *fd* forms a cholesteric instead of a nematic phase. Cholesteric and nematic phases are locally identical to each other. It often takes many days after sample preparation for the *fd* solution to form a fully twisted cholesteric phase. This indicates that the free-energy difference between these two structures is very small. Therefore, we expect that the Onsager theory equally well describes the isotropic–nematic and isotropic–cholesteric phase transitions. In this chapter we use the terms "nematic" and "cholesteric" interchangeably depending on the particular context. Often, when confined to small droplets, such as tactoids observed at the isotropic–cholesteric coexistence, the cholesteric phase is unable to develop and the sample remains nematic.

1.3.1
Properties and Preparation of Filamentous Bacteriophage

The structure of the bacteriophage *fd* is very simple, with a self-assembled hollow cylindrical shell composed of roughly 2800 copies of a single coat protein pVIII. A single circular strand of DNA is enclosed within this hollow shell. The length of the whole virus is determined by the length of the DNA. The ends of the assembly are covered with end-capping proteins, which are different from the major coat protein pVIII. In addition, the two ends are different from one another, which makes *fd* a polar colloid. This characteristic can be used to label each end selectively (Lee et al. 2002).

The physical characteristics of the *fd* virus are a contour length of 880 nm, bare diameter of 6.6 nm, and aspect ratio $L/D_{\mathrm{sc}} \approx 130$. The semi-flexibility of the virus is characterized by the persistence length, $l_{\mathrm{p}} = 2.2$ μm, which has been reported to change with temperature (Tang and Fraden 1996). The colloidal stability of the virus is preserved due to the fact that it has a very high negative surface charge at pH 8.0 (Zimmermann et al. 1986). For a more comprehensive list of most of the known physical constants of *fd*, the reader is referred to the review article by Fraden (1995).

There are well-established methods for growing bacteriophage *fd* and closely related M13 (Maniatis et al. 2000; Dogic and Fraden 2001). In brief, one first grows a large quantity of *Escherichia coli* host. Once the host strain reaches log phase, it is infected with viruses at a well-defined multiplicity of infection (MOI) and the culture is grown for an additional eight hours. The bacterium is separated from the culture by centrifugation at low speed, and the virus in the supernatant is concentrated by adding a neutral polymer, such

as poly(ethylene glycol) (PEG, molecular weight $M_w = 8000$), which acts as a depleting agent. In principle, it is possible to purify the virus further using a cumbersome CsCl gradient centrifugation step. In practice, we found that a two-step sequence of low-speed and high-speed centrifugation produces *fd* virus of sufficient purity for most of our experiments. Once grown, *fd* should be kept in a low-ionic-strength buffer at 4°C. Under these conditions, the solution should be stable for at least a year, although it is difficult to prevent microbial growth over such a long time period even in the presence of sodium azide. Therefore, before use of the virus, we dialyze it against fresh buffer and spin-down aggregates and bacterial debris using a low-speed centrifugation step. The usual yields are about 15–20 mg per liter of infected *E. coli* culture.

There is a tendency for all viruses to form a multimeric structure with a contour length that is an integer multiple of the length of wild-type *fd*. We have found that it is important to choose the appropriate *E. coli* host strain in order to reduce the number of multimers. Although recA$^+$ strains such as JM101 grow faster and produce higher yields of virus, we found that these hosts have a tendency to form dimer and multimer viruses. These can easily be identified once the viruses are labeled and visualized using fluorescence microscopy. Viruses purified from recA$^+$ host form smectic phase at different concentrations when compared to viruses purified form recA$^-$ strains such as Xl1-Blue. In addition, many other structures, such as the lamellar phase described in Section 1.6, are not observed in an *fd* virus grown in recA$^+$ strains. This is presumably due to increased polydispersity of the virus.

It is difficult to assess the polydispersity of the virus. It has a pronounced tendency to break or aggregate during preparation of grids for electron microscopy. It is possible to run agarose gel electrophoresis on whole viruses that are stained with Commassie Blue protein stain (Griess et al. 1990). However, sometimes longer *fd* does not easily enter the gels. It is also possible to strip the virus of its protein and run DNA gel electrophoresis, which is subsequently stained with ethidium bromide. Recently, we have prepared *fd* viruses labeled with the fluorescent dye Alexa 488 (Molecular Probes), which appear very bright when viewed via fluorescence microscopy. These could be used to quantify the polydispersity of the virus. When labeled at very high fraction with Alexa 488 (Molecular Probes) dye, we do not observe any aggregation over a period of a year. In contrast, if the viruses are labeled with larger and more hydrophobic dyes, such as tetramethyl rhodamine (TAMRA), they aggregate into bundles over a period of days. With the proper use of anti-bleaching solution, it is possible to observe Alexa 488-labeled viruses continuously for 5–10 min under full illumination with a 100 W mercury lamp. Figure 1.5 shows a fluorescent microscopy image of Alexa 488-labeled recA$^+$ *fd*. It is easy to observe a number of *fd* with a contour length much longer than that of wild-type *fd*.

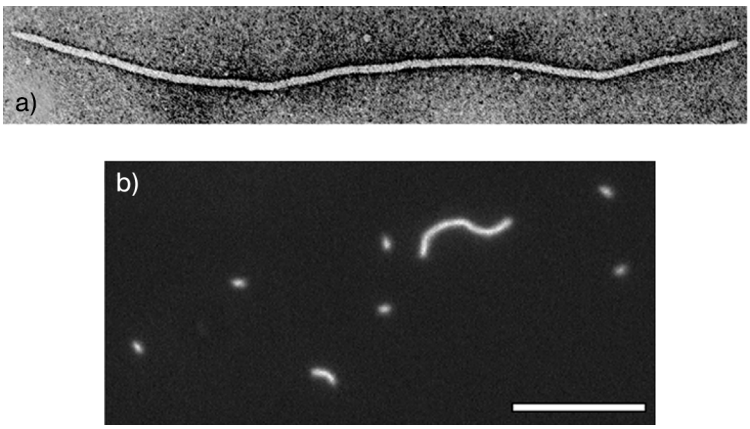

Fig. 1.5 (a) Electron microscope image of a bacteriophage *fd*. The contour length of the virus corresponds to 0.9 μm. (b) Image of a dilute isotropic solution of *fd* confined to a chamber of approximately 1 μm thickness. The presence of *fd* with much larger contour length than the wild type is easily seen. The *fd* was grown in recA$^+$ strain (JM101) and labeled with Alexa 488 (Molecular Probes). The image was taken with a fluorescent microscope equipped with a cooled charge-coupled device (CCD) camera (CoolSnap HQ, Roper Scientific). The scale bar indicates 10 μm. (From Model and Russel, 1988).

All the available data point to the fact that the contour length of *fd* is determined by the size of its DNA. Therefore, it is possible to alter the length of the *fd* by simply adding additional DNA into the *fd* genome using standard recombinant DNA techniques. A few decades ago *fd* with different contour lengths were genetically engineered and used to study the rotational diffusion of rod-like colloids with varying aspect ratio (Maguire et al. 1980). However, this potentially powerful method was not pursued any further. Using similar methods, mutants up to 5 μm long have been described in the biological literature (Herrmann et al. 1980). We have tried to reproduce this method, but have found that, during a large-scale preparation involving many generations of bacterial division, foreign DNA is easily expelled. The resulting culture quickly reverts back to wild-type *fd*. We have had more success in creating mutant *fd* using the phagemid methods, as described in detail in Sambrook et al. (1989). The resulting *fd* are sufficiently monodisperse to form a smectic phase, as shown in Fig. 1.16. For more details, the reader is referred to Dogic and Fraden (2001).

1.3.2
Isotropic–Cholesteric Phase Transition in *fd* Virus Suspensions

Due to the entropic nature of the *fd* suspension, the only variable that determines the phase behavior is the density of the constituent rods. Therefore, with increasing *fd* concentration, an isotropic suspension of *fd* undergoes a first-order phase transition to the nematic/cholesteric phase. It follows that the density of the cholesteric phase is higher than that of the isotropic phase in a coexisting sample. The denser cholesteric phase slowly sediments to the bottom of the sample container, resulting in a macroscopically phase-separated sample (Fig. 1.6).

Recently we compared the experimental results of the isotropic–cholesteric (I–Ch) transition quantitatively to the predictions of the Onsager theory (Tang and Fraden 1996; Purdy and Fraden 2004a). To accomplish this, it is necessary to take into account both the charge and the flexibility of an *fd* virus. It is possible to describe the thermodynamic behavior of a dilute suspension of charged rods using the concept of effective diameter, D_{eff}, as explained in Section 1.2.2, where D_{eff} for *fd* is plotted for three different surface charges (Fig. 1.1). Due to the nonlinear nature of the Poisson–Boltzmann equation, changing the surface charge by an order of magnitude has minimal effect

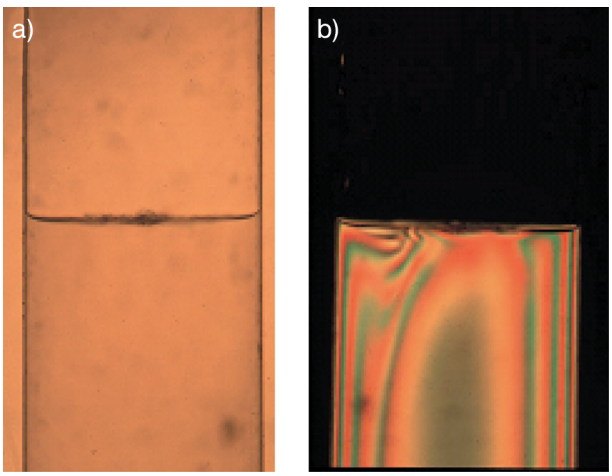

Fig. 1.6 The bulk phase separation between isotropic and nematic phases observed in a TMV suspension. The image on the left is taken with white light, while the image on the right is taken between crossed polarizers. Since the difference in density between the nematic and isotropic phases can be up to 30% over a period of days, the nematic phase sediments to the bottom. The phase diagram for TMV suspension is shown in Fraden et al. (1989). Identical bulk phase separation is observed in *fd* suspension. By measuring the concentration of the virus in coexisting phases, it is possible to determine a phase diagram such as the one shown in Fig. 1.7.

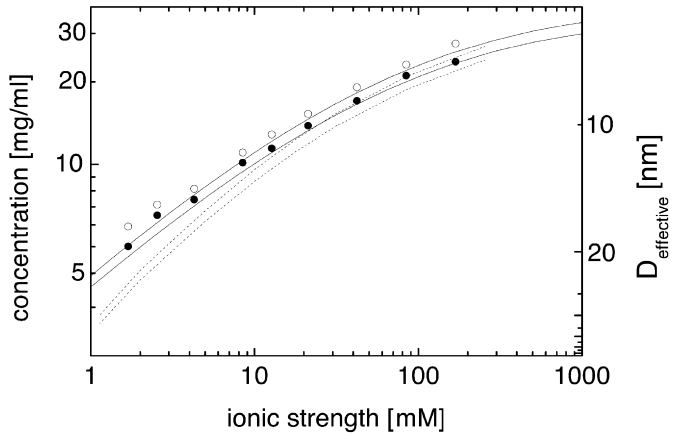

Fig. 1.7 The I–Ch coexistence concentrations measured in an aqueous suspension of *fd* virus as a function of the ionic strength (Tang and Fraden 1995). The full lines are the numerical solution of Chen (1993) for the I–Ch coexistence, which treats excluded-volume interactions at the second virial level while the orientational distribution function is calculated numerically. The dashed lines are the scaled particle theory solution for the I–Ch coexistence in which all virial coefficients are included in an approximate way and the orientational distribution function has an approximate form given by Eq. (1.7). The scale on the right-hand side indicates the effective diameter for a given ionic strength. (From Tang and Fraden, 1996).

on the resulting $D_{\rm eff}$. The flexibility is included according to the prescription given by Khokhlov and Semenov, and discussed in more detail in Section 1.2.3.

Figure 1.7 shows that, with increasing ionic strength, the location of the I–Ch phase transition shifts to higher concentrations. However, increasing ionic strength increases $L/D_{\rm eff}$, which in Onsager theory should decrease the volume fraction of the rods at the I–N transition. The discrepancy can easily be understood if one looks at the condition for instability of the isotropic phase: $(4/\pi)L^2 D_{\rm eff}(N/V) = 4$. The concentration in Fig. 1.7 is not proportional to the effective volume fraction, but to the number density of the virus. If $D_{\rm eff}$ is decreased with the length of the rod remaining constant, it follows that the number density of the virus at the transition has to increase so that the condition for the nematic/cholesteric instability is still satisfied. The experimental data points are compared to the numerical solution of Chen (1993), who approximates the excluded-volume interaction by the second virial coefficient and treats the ODF in an accurate numerical way. We have also plotted the result of a theory in which higher virial coefficients have been taken into account within the scaled particle theory while the orientational degrees of a semi-flexible polymer confined by the nematic field is approximated using the approximation described in Section 1.2.3.

At first sight the agreement between the theory due to Chen and the experiment as shown in Fig. 1.7 is quite good. However, there is reason to

believe that this agreement is fortuitous at low ionic strength. For example, at 1 mM ionic strength, $D_{\text{eff}} \approx 60$ nm, which results in the aspect ratio $L/D_{\text{eff}} \approx 15$. Figure 1.3 clearly shows that for these small aspect ratios third and higher virial coefficients cannot be ignored. Indeed, the results of the scaled particle theory, which include these higher coefficients, predict that the I–N(Ch) transition is located at significantly lower concentration than that found by the experiments and Chen's theory. The agreement between the scaled particle theory, experiments, and Chen's theory is much better at high ionic strength where the effective aspect ratio is large (at 100 mM ionic strength, $L/D_{\text{eff}} \approx 83$), and therefore the excluded-volume interactions are more accurately approximated by the second virial coefficient.

We note that the results from the scaled particle theory shown in Fig. 1.7 should also be treated with a degree of skepticism. To compare the scaled particle theory with experiments on charged rods, we use the effective diameter of the rod. However, the concept of D_{eff} introduced in Eq. (1.13) is only rigorously justified for conditions for which the second virial coefficient is quantitatively valid. There has been a recent theoretical attempt to extend the scaled particle theory to charged particles (Kramer and Herzfeld 1999; Kramer and Herzfeld 2000). Unfortunately, this theory does not extrapolate to Onsager theory for dilute rods, in contrast to the scaled particle theory for hard rods. We also note that the twisting factor ignored in our treatment of D_{eff} for *fd* is strongest at low ionic strength (Stroobants et al. 1986). This effect displaces the I–N(Ch) transition to higher densities.

The effect of the contour length of M13 virus on the I–Ch phase transitions has also been measured (Purdy and Fraden 2004a). Mutant viruses of various contour lengths have been prepared using molecular cloning as described in Section 1.3.1. Figure 1.8 shows the location of the I–Ch phase transition as a function of contour length in terms of the dimensionless concentration $b_{\text{eff}} c_i$. The Onsager theory predicts that the location of the I–Ch will occur when $b_{\text{eff}} c_i \approx 4$. In these units the location of the phase transition is independent of the aspect ratio of the rods, as indicated by the dashed line. Including finite flexibility significantly shifts the location of the I–Ch phase transition to higher concentration, as indicated by the full line. The I–Ch phase transition at high ionic strength, indicated by filled triangles, agrees well with these predictions. However, as the ionic strength decreases to 10 mM, there is a significant deviation between experiment and theory.

Another important parameter that characterizes the I–Ch phase transition is the order parameter of the nematic/cholesteric phase at coexistence. Figure 1.9 shows the behavior of the nematic order parameter as a function of both the contour length and the ionic strength. The order parameter can be extracted from birefringence measurements once the birefringence per particle is measure using X-ray scattering as described in Section 1.3.5 and Purdy